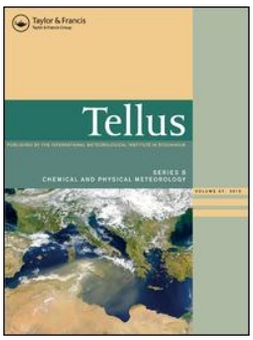

Tellus B: Chemical and Physical Meteorology

ISSN: (Print) 1600-0889 (Online) Journal homepage: https://www.tandfonline.com/loi/zelb20

Ozone exchange within and above an irrigated Californian orchard

J.S. Brown, M.M. Shapkalijevski, M.C. Krol, T. Karl, H.G. Ouwersloot, A.F. Moene, E.G. Patton & J. Vilà-Guerau de Arellano

To cite this article: J.S. Brown, M.M. Shapkalijevski, M.C. Krol, T. Karl, H.G. Ouwersloot, A.F. Moene, E.G. Patton & J. Vilà-Guerau de Arellano (2020) Ozone exchange within and above an irrigated Californian orchard, Tellus B: Chemical and Physical Meteorology, 72:1, 1-17, DOI: 10.1080/16000889.2020.1723346

To link to this article: https://doi.org/10.1080/16000889.2020.1723346

Published online: 11 Feb 2020.

Tellus SERIES B CHEMICAL AND PHYSICAL METEOROLOGY
PUBLISHED BY THE INTERNATIONAL METEOROLOGICAL INSTITUTE IN STOCKHOLM

Ozone exchange within and above an irrigated Californian orchard

By BY J.S. BROWN[1], M.M. SHAPKALIJEVSKI[1,2]*, M.C. KROL[1], T. KARL[3], H.G. OUWERSLOOT[4], A.F. MOENE[1], E.G. PATTON[5], and J. VILÀ-GUERAU DE ARELLANO[1],
[1]*Meteorology and Air Quality Section, Wageningen University, Wageningen, The Netherlands;* [2]*Department of Mathematics and Computer Sciences, Freie Universität, Berlin, Germany;* [3]*Department of Atmospheric and Cryospheric Sciences, University of Innsbruck, Innsbruck, Austria;* [4]*Department of Atmospheric Chemistry, Max Planck Institute for Chemistry, Mainz, Germany;* [5]*Mesoscale and Microscale Meteorology Lab, National Center for Atmospheric Research, Boulder, CO, USA*

(Manuscript Received 3 August 2018; in final form 13 December 2019)

ABSTRACT

In this study, the canopy effects on the vertical ozone exchange within and above Californian orchard are investigated. We examined the comprehensive dataset obtained from the Canopy Horizontal Array Turbulence Study (CHATS). CHATS typifies a rural central Californian site, with O_3 mixing ratios of less than 60 ppb and moderate NO_x mixing ratios. The CHATS campaign covered a complete irrigation cycle, with our analysis including periods before and after irrigation. Lower O_3 mixing ratios were found following irrigation, together with increased wind speeds, decreased air temperatures and increased specific humidity. Friction velocity, sensible heat and gas fluxes above the canopy were estimated using variations on the flux-gradient method, including a method which accounts for the roughness sublayer (RSL). These methods were compared to fluxes derived from observed eddy diffusivities of heat and friction velocity. We found that the use of the RSL parameterization, which accounts for the canopy-induced turbulent mixing above the canopy, resulted in a stronger momentum, heat, and ozone exchange fluxes above this orchard, compared to the method which omits the RSL. This was quantified by the increased friction velocity, heat flux and ozone deposition flux of up to 12, 29, and 35% at 2.5 m above the canopy, respectively. Within the canopy, vertical fluxes, as derived from local gradients and eddy diffusivity of heat, were compared to fluxes calculated using the Lagrangian inverse theory. Both methods showed a presence of vertical flux divergence of friction velocity, heat and ozone, suggesting that turbulent mixing was inefficient in homogenizing the effects driven by local sources and sinks on vertical exchange of those quantities. This weak mixing within the canopy was also corroborated in the eddy diffusivities of friction velocity and heat, which were calculated directly from the observations. Finally, the influence of water stress on the O_3 budget was examined by comparing the results prior and after the irrigation. Although the analysis is limited to the local conditions, our *in situ* measurements indicated differences in the O_3 mixing ratio prior and after irrigation during CHATS. We attribute these O_3 mixing ratio changes to enhanced biological emission of volatile organic compounds (VOCs), driven by water stress.

Keywords: roughness-sublayer, monin-obhukov similary theory, ozone, canopy

1. Introduction

Tall vegetation accounts for around 31% of the total land cover (Simard et al., 2011) and plays a vital role in regulating the climate on a local and global scale (Bonan, 2008). Tall vegetation is considered any canopy with an average height greater than a few meters, encompassing coniferous and deciduous forests as well as agricultural orchards and crops. These vegetation systems connect the terrestrial biome and the atmosphere by continuously cycling energy, water, carbon dioxide and chemically

*Corresponding author. e-mail: metoshapkalijevski@gmail.com

Citation: Tellus B: 2020, **72**, 1445379, https://doi.org/10.1080/16000889.2020.1723346

reactive species (Gao et al., 1989). This exchange can alter both the physical and the chemical properties of the planetary boundary layer (PBL) and as such it is critical to gain a comprehensive understanding of the mechanisms driving this exchange. These mechanisms, in the case of the exchange of reactive compounds, involve interaction between biogenic emissions, deposition, chemistry and turbulent transport (Jacobson, 2005; Seinfeld and Pandis, 2016). Due to its relevance in atmospheric chemistry, deposition of ozone (O_3) is an important removal mechanism. Thus, it is necessary to study which effects need to be accounted for to improve the representations of ozone deposition within and above tall canopies.

Observations of the exchange processes between tall vegetation and the atmosphere have traditionally consisted of direct measurements within and above canopies using eddy covariance (EC) flux towers (e.g. Baldocchi et al., 2001). When considering trace-gas fluxes, for which fast-response analysers for various reactive gas species are often unavailable, the flux-gradient method is used to determine fluxes within and above the canopy. The flux-gradient method relates the vertical concentration profile of a scalar to vertical fluxes through a turbulent transfer coefficient (Stull, 1988). However, it is recognised that standard flux-gradient methods are only valid well above vegetated surfaces due to the presence of the roughness sublayer (RSL) (Raupach, 1979). The RSL normally extends 2–3 times the canopy height (e.g. Thom et al., 1975; Garratt, 1980; Högström, 1988; Cellier and Brunet, 1992) and is the area where the turbulent structure is strongly influenced by the individual roughness elements (Raupach et al., 1996). This altered turbulent mixing in the RSL leads to enhanced turbulent transport of momentum, heat and moisture relative to transport predicted by standard flux-gradient theory (Iwata et al., 2010; Shapkalijevski et al., 2016). Various authors have attempted to account for the presence of the RSL in the flux-gradient relationship for momentum and heat fluxes (e.g. Garratt, 1980; Cellier and Brunet, 1992; Physick and Garratt, 1995; Mölder et al., 1999; Harman and Finnigan, 2007, 2008; De Ridder, 2010). Shapkalijevski et al. (2016) used the methods outlined in Harman and Finnigan (2007, 2008) as the 'state of the art' method of accounting for the RSL effects when analysing turbulent parametrizations of momentum, heat and moisture above an orchard canopy.

But the presence of tall canopy not only affects the exchange of momentum and energy between the vegetation and the atmosphere; it also influences the reactive-gas exchange by altering the emission/deposition fluxes, as well as the vertical turbulent transport of those reactants. Therefore, in this study we investigate the influence of the tall vegetation on the vertical exchange of reactive compounds, mainly focusing on the vertical ozone exchange. To determine the effects of the canopy-induced turbulent mixing on the vertical fluxes of ozone above the canopy, we study the influence of accounting for the RSL effects when deriving those fluxes from observed ozone mixing ratio. Within the canopy we validate the locally-derived gradient method for flux retrieval by comparing it to a flux-retrieval approach, based on the Lagrangian inverse theory (Raupach 1989a), that accounts for a non-local turbulent transport.

To this end, we analyse the observations gathered during the Canopy Horizontal Array Turbulence Study (CHATS). The CHATS campaign took place in spring 2007 in central California, with the aim of collecting a dataset to improve the understanding of vegetation, atmosphere, and land-surface interactions (Patton et al., 2011). The CHATS dataset includes detailed vertical profiles of micrometeorological variables and trace gas mixing ratios. The CHATS observations were collected during complete irrigation cycle of the orchard. This allows the comparison between water availability regimes and an examination of the relationship between water stress, plant emissions and the chemical regime at CHATS.

By presenting the general micrometeorological and chemical characteristics observed at CHATS, we aim at providing answers to the following specific questions:

1. What is the relevance of canopy-induced turbulence in the representation of ozone exchange (vertical turbulent fluxes) above the orchard?
2. How does ozone vertical exchange respond to situations characterized by water stress?

The article is structured as follows: Section 2 describes the CHATS site, data treatment, and the methods and formulas used to infer fluxes from observed mean gradients. Section 3 discusses the general meteorological and chemical conditions of the CHATS site. Section 4 examines the validity of RSL adapted flux-gradient methods and presents the calculated fluxes and deposition velocities of O_3 and NO_x. Section 5 discusses the assumption of non-reactivity used when calculating fluxes and examines the differences in O_3 mixing ratios before and after irrigation of the orchard.

2. Methods

2.1. Observations and data treatment

The CHATS experimental site was situated in a mature walnut (Paradox Hybrid; *Juglans californica* x *Juglans regia*) orchard near Dixon, California (N 38° 29′15″, W

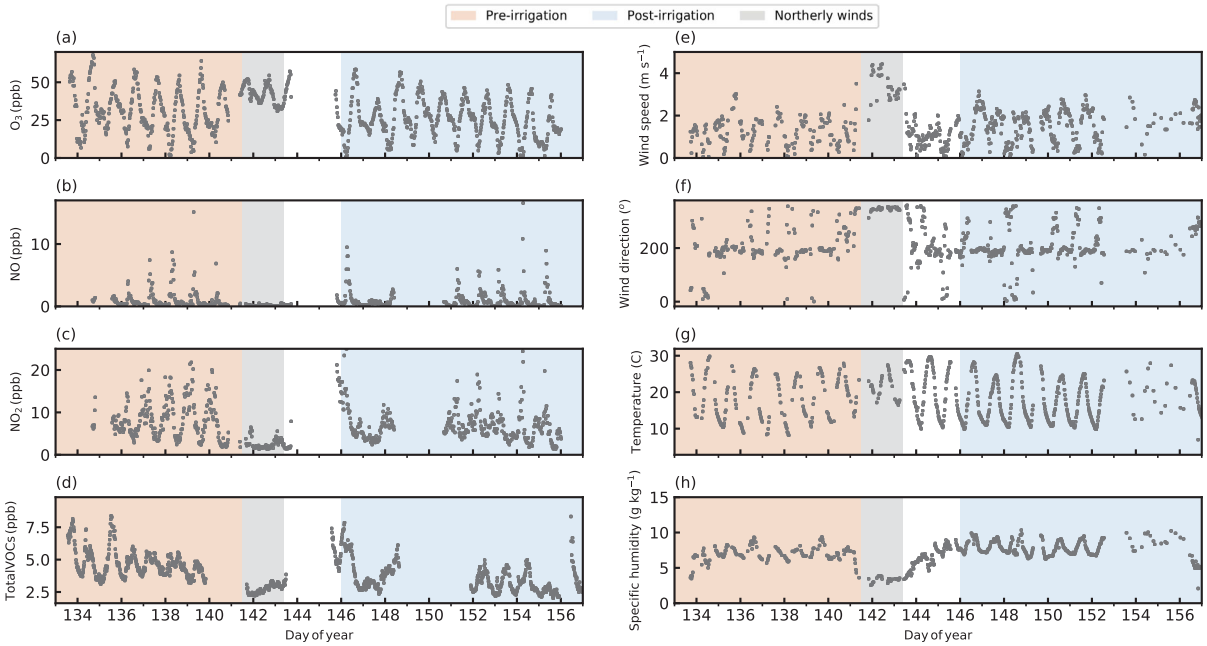

Fig. 1. Timeseries of gas concentrations and meteorological conditions, taken at 11 m above the ground surface (1 m above the canopy) between 13 May and 5 June 2007. The orange shaded area indicates the pre-irrigation period (13–21 May), while the blue shaded area shows the post-irrigation period (26 May–5 June). The gray shaded area (20 May at noon to 22 May at noon) represents the period with 'northerly' winds.

121° 50′45″). The trees were located roughly 7 m apart with an average height of 10 m (Patton et al., 2011). The campaign consisted of three 4-week phases (Patton et al., 2011), with this study focusing on the 3rd phase which followed leaf-out. During the latter portion of the 3rd phase, the orchard was irrigated in a rotating fashion with a complete irrigation cycle taking 6 days (Patton et al., 2011), thereby allowing observations to be grouped into pre-irrigation (13–21 May 2007) and post-irrigation (26 May to 5 June 2007) periods (Fig. 1).

In this study observations from a 30-m tall vertical tower are used. The tower was located near the northern boundary of the orchard, allowing around 800 m of canopy fetch to insure the RSL was fully developed. Therefore, the flux data studied here are predominantly related to southern winds (most common wind direction at CHATS) while for northern winds, with plausible insufficient fetch, no flux data are included. This tower held a variety of instruments for observing turbulence, fast and slow chemistry, aerosols and radiation within and above the canopy. Thirteen sonic anemometers operating at 60 Hz (mounted at 1.5, 3, 4.5, 6, 7.5, 9, 10, 11, 12.5, 14, 18, 23 and 29 m) (CSAT3, Campbell, UK) measured all three wind components and virtual temperature. 12 NCAR-Vaisala hygrothermometers operating at 2 Hz (mounted at 1.5, 3, 4.5, 6, 7.5, 9, 10, 11, 14, 18, 23 and 29 m) (TRH, NCAR, USA) measured aspirated temperature and relative humidity. In addition, at every other level, specific humidity was observed using additional hygrometers (Krypton, Campbell, UK) operating at 20 Hz. Data from the sonic anemometers was rotated using the planar fit method (Wilczak et al., 2001), based on 5 min average velocities. Short gaps (i.e. less than 4 s) in the raw turbulence data of the sonic anemometers and hygrometers were filled by linear interpolation. Incomplete vertical profiles of means, variances, and covariances were filled by vertical interpolation, where the maximum size of a vertical gap was one instrument for hygrometer and two instruments for a sonic or a TRH sensor. See Shapkalijevski et al. (2016) for further information about how the EC data was processed.

Mean concentrations of O_3, NO, NO_2 were obtained at six heights (1.5, 4.5, 9, 11, 14 and 23 m) every 30 min. Ozone concentrations were measured by UV absorbance (2B Technologies, Model 205) every 10 s and then averaged over the entire 5 min sampling time on each level, excluding only the first 15 s to insure adequate flushing of the connecting gas lines (Karl et al., 2008). NO and NO_2 concentrations were measured by vacuum chemiluminescence Eco Physics CLD88Y analyser (Patton et al., 2011). VOC gradient measurements of acetone, benzene, toluene and monoterpenes were taken with a Photon-Transfer

Reaction Mass Spectrometer (PTR-MS), with sequential sampling at 1.5, 4.5, 9, 11, 14 and 23 m, with a 5-second integration time (Karl et al., 2008). In addition, *in situ* identification of methyl salicylate (MeSA) within ambient air was observed using a Gas Chromatograph with Mass Spectrometer (GC-MS, HAPSITE Smart, INFICON, USA) (Karl et al., 2008). Please see Karl et al. (2008) for a detailed description of the O_3 and VOC sampling regime. Detailed information about the campaign setup, site description and instruments used can be found in Patton et al. (2011) and Karl et al. (2008).

Thirty minute mean mixing ratios were used to create daytime diurnal evolutions of each chemical species, for both irrigation periods. We limited our analysis to daytime convective conditions, between 10:00 and 17:00 local time (LT), when atmospheric thermodynamic and inert chemical constituents are assumed to be well mixed in the convective boundary layer. Moreover, by taking 30 minute averages of fluxes and gradients we assume that the majority of scale motions in the convective boundary-layer flow were well captured. The effects of larger then 30 min motions (e.g. acting over several hours) on those gradients and fluxes were not specifically treated in this study.

2.2. Methods for inferring gas fluxes

The flux gradient method, or *K*-theory, can be used to estimate fluxes of compounds when fast (EC) measurements are not available (e.g. Cellier and Brunet, 1992). This theory is a parameterization which relates the vertical flux of a compound, F_c ($F_c \equiv \overline{w'C'}$ in case of eddy cocariance measurements), to its mean concentration (or mixing ratio), $\overline{C}$, through the mean turbulent transfer coefficient for scalars, K_C:

$$F_c(z) = -K_C(z)\frac{\partial \overline{C}(z)}{\partial z}. \quad (1)$$

As Equation 1 is written it is assumed that $\overline{K}_C$ is not influenced by chemistry, although this assumption can be questionable (e.g. Vila-Guerau De Arellano and Duynkerke, 1992) and will be discussed further below. Fluxes of reactive gases are estimated from the observed vertical mixing ratio profiles within and above the canopy by using different adaptations of *K*-theory method. In particular, the transfer coefficient K_C for the vertical fluxes of O_3, NO, and NO_2 were calculated using three different methods:

- K_COBS: using locally observed heat fluxes and potential temperature gradients to estimate K_C
- Monin–Obukhov similarity theory (MOST): parametrization of K_C based on atmospheric stability (ζ expressed as $(z-d)/L$ where z is the height from the ground surface, d is the displacement height and L is the Obukhov length) and semi-empirical flux-gradient relationships.
- MOST + RSL addition: an extension of the MOST method which includes the additional parametrisation for influence of the RSL (Harman and Finnigan 2007, 2008)

In addition to these three methods, the Inverse Localized Near-Field Lagrangian (ILNF) method was used. Using the ILNF method fluxes are related to observed mixing ratios by a combination of diffusive and non-diffusive turbulent transport (Raupach, 1989a). Below these four methods of flux calculation are described in more detail.

In summary, the K_COBS method was used to estimate fluxes of O_3, NO and NO_2 within and above the canopy. The MOST and MOST + RSL were used to calculate fluxes only above the canopy, while the ILNF was used only within the canopy.

2.2.1. K_cOBS. To calculate the vertical flux, the K_COBS method uses Equation 1 together with observations of the vertical flux of the potential temperature, $\overline{w'\theta'}$, and the potential temperature gradients, $d\overline{\theta}/dz$, to calculate the K_C specific to the CHATS site. During CHATS momentum, heat and moisture fluxes were directly measured using EC. We assume that the exchange coefficients of gases are equal to the exchange coefficients for heat (i.e. $K_C(z) = K_\theta(z) = -\overline{w'\theta'}(z)/[d\overline{\theta}/dz]$). To calculate the vertical scalar gradients used within the K_COBS method, the profile of each scalar was fitted to the curve $y = a + b\ln(z) + c\ln(z)^2$ following Mölder et al. (1999). The fitting of the vertical profiles was separated into above (> 10 m) and below canopy (≤ 10 m) (Eq. 1).

2.2.2. MOST. Using the Monin–Obukhov Similarity theory (Monin and Obukhov, 1954), $\overline{K}_C$ can be described as:

$$K_C(z) = \frac{\kappa\ (z-d)\ u_*}{\phi_H(\zeta)}, \quad (2)$$

where κ is the von Kármán constant ($\kappa = 0.41$), u_* is the friction velocity, ϕ_H is dimensionless universal stability function of heat (Högström, 1988). To be consistent with the K_COBS method, we again use the stability function of heat as a proxy for the exchange coefficients of the reactive gases. While the displacement height, d, varies with atmospheric stability (e.g. Harman and Finnigan, 2007, 2008; Shapkalijevski et al., 2016) a constant value of d equal to 7.6 m was applied (Shapkalijevski et al., 2016) for both MOST and MOST + RSL as we focus only on

convective cases. We have also ignored chemistry's potential influence on d (e.g. Patton et al., 2001).

The MOST method assumes horizontally homogeneous flow and far-field diffusion (Stull, 1988). When combining and integrating Eq. 2 and Eq. 1 between two heights z_1-d and z_2-d above the canopy (Moene and Van Dam, 2014), the vertical flux becomes:

$$F_C = \frac{\kappa\ u_*\ [\overline{C}(z_2-d)-\overline{C}(z_1-d)]}{\ln\left(\frac{z_2-d}{z_1-d}\right)+\psi_H(\zeta_1)-\psi_H(\zeta_2)}, \quad (3)$$

where ψ_H is the integrated form of ϕ_H. The forms of ϕ_H and ψ_H used in this study are based on Högström (1988) and Paulson (1970). ζ_1 and ζ_2 are atmospheric stability at the two heights above the canopy.

2.2.3. MOST + RSL. To correct the standard similarity flux-gradient relationships for the presence of the RSL, we follow Harman and Finnigan (2007, 2008). The effects of the RSL appear through the inclusion of the additional function, $\hat{\phi}_H(\zeta,\ \delta_\omega)$, to Eq. 2:

$$K_C(z) = \frac{\kappa\ (z-d)\ u_*}{\phi_H(\zeta)\ \hat{\phi}_H(\zeta,\ \delta_\omega)}, \quad (4)$$

where δ_ω is the canopy-top vorticity thickness, a characteristic length scale in the RSL representing the length of the turbulent mixing eddies formed at the canopy-atmosphere interface due to the presence of an inflection point in the mean wind at the canopy top (Finnigan et al., 2009). δ_ω is defined as the ratio between the mean horizontal wind speed and its gradient at the canopy top ($\delta_\omega = \overline{u}/[d\overline{u}/dz]$) (Raupach et al., 1996; Harman and Finnigan, 2007), and is dependent on canopy density and atmospheric stability. For sparse canopies under near-neutral conditions, Raupach et al. (1996) found that $\delta_\omega \simeq 0.5h_c$, where h_c is the canopy height. This is corroborated by observations of the wind speed and its gradient during the CHATS experiment following leaf-out for the majority of stability classes (see Fig. 5 in Shapkalijevski et al., 2016). By including Eq. 4, the integrated version of Eq. 1 then becomes:

$$F_C = \frac{\kappa\ u_*\ [\overline{C}(z_2-d)-\overline{C}(z_1-d)]}{\ln\left(\frac{z_2-d}{z_1-d}\right)+\psi_H(\zeta_1)-\psi_H(\zeta_2)-\hat{\psi}_H(\zeta_1,\delta_\omega)+\hat{\psi}_H(\zeta_2,\delta_\omega)}. \quad (5)$$

The function $\hat{\psi}_H(\zeta,\delta_\omega)$ is the highly non-linear integral function of $\hat{\phi}_H(\zeta,\ \delta_\omega)$ solved by numerical integration (see Harman and Finnigan, 2007, 2008).

2.2.4. ILNF. The ILNF theory assumes that within the canopy turbulent transport of scalar quantities (i.e. heat, water, gases) is a combination of both diffusive and non-diffusive (remotely driven) processes due to the changes in turbulence structure near and within rough surfaces (Raupach, 1989a; Finnigan et al., 2009). To include these effects, Raupach (1989a) proposed the ILNF theory to combine the influence of near-field and far-field turbulent transport on turbulent transport. In the ILNF method, the source profile, $S(z)$, is related to the observed mixing ratio profiles $C(z)$ via a dispersion matrix $\mathbf{D}_{ij}$:

$$C_i-C_r = \sum_{j=1}^{m} \mathbf{D}_{ij}\ S_j\ \Delta z_j \quad (6)$$

where C_i is the measured mixing ratio of a scalar quantity within and above the canopy at certain level i ($i = 1, 2, .., n$), and at certain moment in time, relative to the uppermost measured reference mixing ratio, C_r, above the canopy. The index j refer to levels of the scalar source/sink distribution within the canopy ($j = 1, 2, .., m$), which are different to the levels of the concentration profiles (see Fig. 7 in Raupach, 1989a). n and m represent the number of mixing ratio and flux levels respectively, with the condition that $m < n$. This dispersion matrix $\mathbf{D}_{ij}$ depends on the standard deviation of the vertical velocity variance, σ_w, and the Lagrangian integral time scale T_L. σ_w and T_L were calculated based on Raupach (1989b, Eq. 49), scaled by friction velocity and canopy height from the CHATS site. Since these quantities are height dependent, we have normalized the profiles of σ_w and T_L by using locally calculated u_* at each measurement level over 30 min. Although the theoretical formulation of σ_w and T_L by Raupach (1989b) was given for neutral atmospheric conditions, we have applied it (with satisfactory results, see later Section 4) for the moderate-convective to near-neutral condition at CHATS (Dupont and Patton, 2012; Shapkalijevski et al., 2017). For studies that treat whole range of stability conditions explicitly, or extreme stability (e.g. free convection, very stable stratification), it is relevant to note that T_L varies with atmospheric stability (e.g. Gerken et al., 2017). By solving Eq. 6 for S_i, the flux of a scalar can then be found via:

$$F(z) = \int_0^z S(z)\ dz, \quad (7)$$

where z = 0 is the ground surface below the canopy. An important improvement of the ILNF method is that it can account for counter-gradient fluxes (Denmead and Bradley, 1987; Raupach, 1989b). Detailed information about the ILNF theory can be found in Raupach (1989a). The ILNF method of flux calculation was used to estimate fluxes of O_3, NO and NO_2 at 2, 4, 6 and 8 m within the canopy.

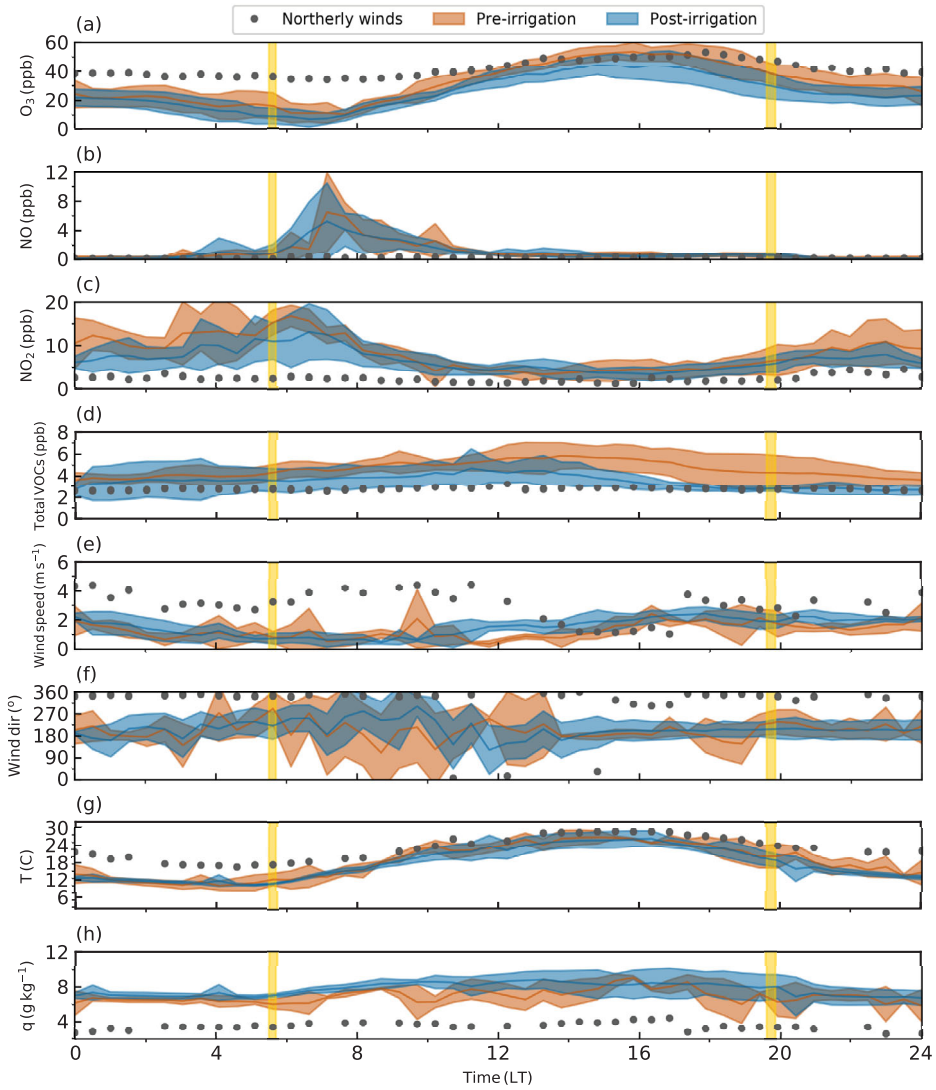

Fig. 2. Mean diurnal evolution of (a) O_3, (b) NO, (c) NO_2, (d) total VOC mixing ratios, (e) wind speed, (f) wind direction, (g) temperature and (h) specific humidity at 11 m above the ground (1 m above the canopy) for the pre-(orange) and post-(blue) irrigation periods. The vertical shaded areas indicate sunrise and sunset times for Davis, including both the 'Northerly winds', pre- and post-irrigation periods. The shaded area represents the standard error of the mean.

3. Combined characterisation of chemistry and meteorology during CHATS

The CHATS site shows meteorological conditions typical of a Mediterranean climate, with the average daily temperature during the campaign peaking at 26 °C by 15:00 LT, and the average daily specific humidity reaching a peak of 8.6 g kg^{-1} (Figs. 1 and 2).

Figure 1 shows the timing of the pre- and post-irrigation periods. In addition to these two irrigation periods, between days 141 and 144 (20th May–23rd May 2007) the wind regime changes from prevailing southerly winds to winds from the north. We refer to this period as the 'northerly winds' period. Outside the 'northerly winds' period, winds were generally from the south. During the 'northerly winds' period increased wind speeds of up to 5.5 m s^{-1}, together with the advection of warm, dry air and a suppression of morning NO_x mixing ratio peaks (Figs. 2b, c, 3e, g, h) were observed. Wind speeds above the canopy increased following irrigation, reaching mean (per period) magnitude of 3.8 m s^{-1} at 23 m (Fig. 3e). Wind direction before and after irrigation were very similar, with no wind rotation with height (Fig. 3f). The mean temperature prior to irrigation was around 1 °C higher than after irrigation (Fig. 3g). Mean (per period) specific humidity showed a peak within and below the canopy both before and after irrigation, indicative of

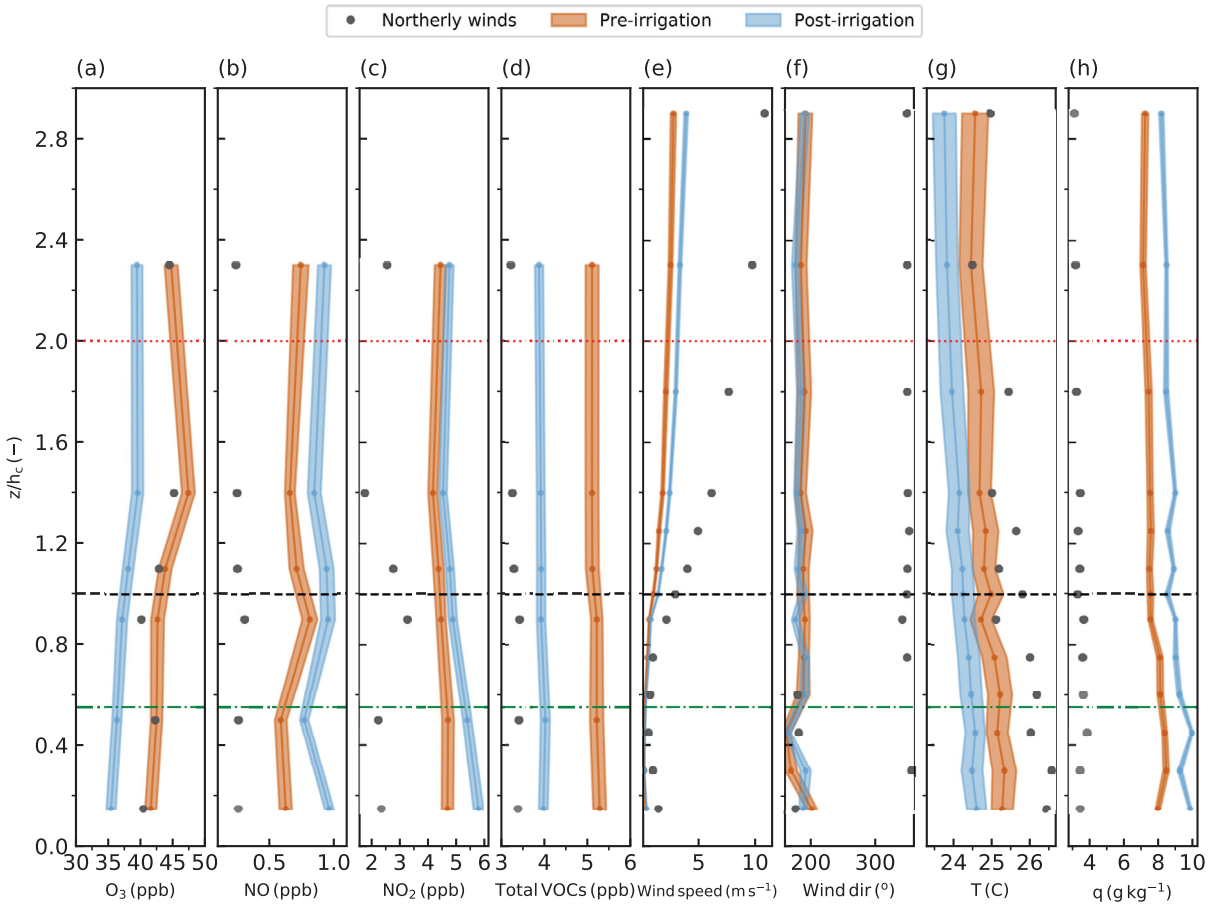

Fig. 3. Vertical profiles of (a) O_3, (b), NO, (c) NO_2, (d) total VOC mixing ratios, (e) mean wind speed, (f) wind direction, (g) temperature, and (g) specific humidity, averaged between 10:00 and 17:00 LT for the 'Northerly winds', pre-(orange) and post-(blue) irrigation periods. The green dashed line indicated the bottom of the canopy, the black dashed line indicates the canopy crown and the red line indicates the approximate height of the roughness sublayer. The shaded areas are the standard error of the means.

transpiration by the vegetation, with increases of 2 g kg^{-1} following irrigation (Fig 3h). The remote sensing observations using lidar over CHATS (http://lidar.csuchico.edu/lgd/nsf_results) showed a deeper boundary-layer (up to 1200 m maximum daily) prior to irrigation compared to a shallower boundary layer (up to 700 m maximum daily) following irrigation.

The O_3 diurnal cycle reaches a peak at around 15:00 LT, following daytime ozone production and entrainment from the overlying free atmosphere (Fig. 2a). The O_3 minimum coincides with the peak in NO_x mixing ratios at 07:00 LT. O_3 mixing ratios before irrigation are consistently higher than after irrigation, with this increase being more pronounced during the daytime. The O_3 mixing ratios here are comparable to other rural regions in Central California during spring, with Fares et al. (2012) finding O_3 mixing ratio above a Californian orange orchard of around 55 ppb in spring 2009, with daytime peaks in the summer exceeding 100 ppb.

NO and NO_2 peak at around 07:00 LT due to accumulation of fresh emissions in the shallow night-time boundary layer and the lack of photochemistry (Fig. 2b, c). At sunrise, NO_2 photolysis begins and starts cycling between NO and NO_2 (Seok et al. 2013) which leads to the morning build-up of NO before the boundary layer begins to grow and to dilute the NO_x mixing ratios. The mean NO_x mixing ratios during CHATS are similar to findings by (Murphy et al., 2007) who found Californian daytime mean mixing ratios of NO_x to be between 5 and 18 ppb, with high NO_x levels resulting mainly from traffic emissions. It is likely that traffic emissions are the dominant source of NO_x at the CHATS site, which is situated 3 km north of a busy highway and the town of Dixon and generally receives winds from the south (Fig. 2f). During the 'northerly winds' period, when the source area for the CHATS site became dominated by agricultural fields, both NO and NO_2 were significantly reduced (Fig. 2b, c). However, this is only a plausible explanation and will

require a denser spatial coverage of NO_x measurements and soil emissions observations to better characterize the advective contributions.

Mixing ratios of total VOCs were higher before irrigation (Fig. 2d). The largest contributor to the total measured VOC mixing ratio was acetone, with mixing ratios reaching 5 ppb before irrigation, while the contributions of all other VOCs were less than 0.5 ppb individually. While benzene and toluene showed no clear diurnal pattern, acetone, monoterpenes and MeSA all showed a diurnal pattern, with peak mixing ratios in the afternoon (not shown). In addition to this afternoon peak, a second smaller morning peak was seen in monoterpenes and MeSA mixing ratios. Significant mixing ratios of MeSa were observed (0.1 ppb) during CHATS, although typical mixing ratios of MeSA remain uncertain (Karl et al., 2008).

Figure 3 shows the vertical profiles of key gases and meteorological variables, averaged between 10:00 and 17:00 LT (i.e. during convectively dominated daytime conditions). The maximum O_3 mixing ratio is seen at 14 m, with the difference between O_3 mixing ratios before and after irrigation, equal to 8 ppb, maintained throughout the canopy (Fig. 3a). NO exhibits two peaks in mixing ratio; at the ground surface and at 10 m (just below the canopy crown), with a decrease towards 14 m (Fig. 3b). NO_2 mixing ratios decrease with height consistently throughout the canopy towards 14 m before increasing (Fig. 3c). This NO_x depletion at 14 m indicates a sink of NO_x, with processes other than soil NO emissions and cycling between NO and NO_2 controlling NO_x mixing ratios such as the advection of NO_x or conversion to N_2O_5. Min et al. (2014) examined NO_x mixing ratios above a pine plantation in the Sierra Nevada Mountain range and observed an NO depletion and NO_2 enhancement within the canopy, with a strong dependence on time of day. This shift in the gradient of NO_x at 14 m may indicate this is the region of interface between local sources and advection of large air masses over the CHATS site. Unlike NO_x and O_3 there is no appreciable pattern in total VOC vertical profile, with a consistent 1 ppb decrease in mixing ratio following irrigation (Fig. 3d).

4. Inferring fluxes from gradients at the CHATS site

4.1. Validity of RSL-adapted flux-gradient method at the CHATS site

In order to gain confidence in the methods used for flux calculation (presented in Section 2.2), a validation of those methods is needed. To this end, we compare the calculated fluxes against fluxes of those variables for which we have direct flux observations (through EC)

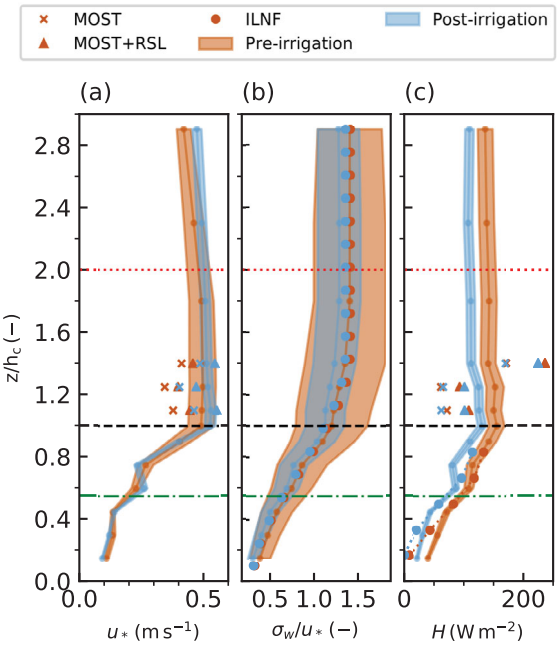

Fig. 4. Observed and calculated vertical profiles of **(a)** friction velocity **(b)** vertical velocity standard deviation (σ_w/u_*) and, **(c)** sensible heat, averaged between 10:00 and 17:00 LT pre-(orange) and post-(blue) irrigation periods. The vertical velocity standard deviation, as calculated from Raupach (1989a) for neutral conditions (solid line), is normalized by the locally calculated u_* from EC observations pre and post irrigation. The shaded area represents the standard deviation of the mean. See Fig 3 for a description of the horizontal lines.

available. The vertical profiles of observed friction velocity (u_*) and sensible heat (H) for the both irrigation periods are compared with calculated u_* and H in Fig. 4 (a, c). The u_* and H above the canopy were calculated as described in Subsection 2.2 using the same procedure as employed in the calculation of the gas fluxes. To convert to sensible heat flux, Eqs. 3 and 5 were multiplied by the air density ($\rho = 1.2$ kg m^{-3}) and the specific heat capacity of air ($C_p = 1005$ J kg^{-1} K^{-1}). In applying these methods and comparing with explicit EC flux calculations, we are able to asses the validity and/or uncertainty of our method.

There is a decrease in sensible heat following irrigation, while friction velocity shows a slight increase following irrigation above the canopy (Fig. 4). The MOST + RSL method improves over the MOST method for both u_* and H at $z/h_c = 1.1$ and 1.25, similar to results previously shown by Mölder et al. (1999) and De Ridder (2010). However, u_* and H calculated at $z/h_c = 1.4$ showed overestimation and sharp positive divergence with respect to the observed u_* and H. This is due to the

higher wind speed at higher levels (one could normalize u_* with mean wind speed (e.g. at canopy top, or at the top of the RSL (Harman and Finnigan, 2007, 2008). The MOST + RSL method provides an improvement for u_* and H, with fluxes estimated by this method being 80% and 61% of observed fluxes (by EC), respectively, compared to 69 and 42 for MOST at $z/h_c = 1.25$ (Table 1). Moreover, the estimated differences of 12% (for u_*) and 29% (H) between MOST + RSL and MOST at $z/h_c = 1.25$ demonstrated and quantified the effects of the canopy-induced turbulence on momentum (u_* used as proxy) and energy (H used as proxy) exchange when estimated from wind speed and potential temperature gradients (Table 1). The two methods (MOST and MOST + RSL) above were applied above the canopy, while the ILNF method was used to estimate sensible heat fluxes within the canopy. Figure 4c shows the performance of the ILNF method (Raupach, 1989a) in calculating the sensible heat fluxes compared to sensible heat observed by EC. The profile of the vertical velocity variance is used as input into the ILNF model. The ILNF method closely reproduces the observed H within the canopy (Fig. 4c). For u_* and H shown in Fig. 4a, c, there is a strong vertical divergence within the canopy, indicating the effects of canopy sources and sinks on the profiles of these variables. Indeed, the lower intensity of turbulent mixing within the canopy, as represented by the eddy diffusivity of momentum and heat Fig. 5, suggested that the canopy sources and sinks dominate the vertical exchange of momentum and heat within the canopy. The stronger turbulent mixing above the canopy (Fig. 5) contributes towards constant vertical fluxes in height (Fig. 4a, b).

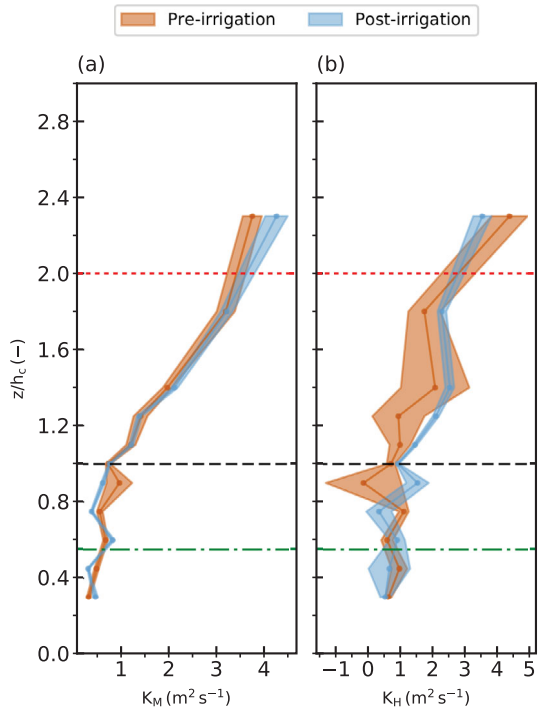

Fig. 5. Mean vertical profiles of eddy diffusivity of **(a)** momentum, and **(b)** heat, averaged between 10:00 and 17:00 LT pre-(orange) and post-(blue) irrigation periods. The shaded area represents the standard deviation of the mean. See Fig. 3 for a description of the horizontal lines.

4.2. Gas fluxes and the ozone exchange

In Section 4.1, we show that when using the MOST and MOST + RSL flux-gradient methods to calculate vertical fluxes of momentum and heat, the MOST + RSL method provides a more precise and robust estimate of fluxes above the canopy. Since there are no direct EC observations of gas fluxes available, we will now infer these fluxes using both methods mentioned above the canopy, as well as the ILNF method within the canopy. Figure 6 shows the vertical profiles of fluxes for the three chemical species, calculated by the four flux-gradient methods. Here, we assume the K_COBS method as a best estimate of the fluxes, with the performance of the other methods being compared to the K_COBS method. Later, in Section 5.1 we discuss the validity of this assumption.

O_3 shows a strong vertical flux divergence, with the largest negative fluxes occurring within and just above the canopy, reaching up to $-2.5\,\mu g\ m^{-2}\ s^{-1}$ (Fig. 6a, d). The positive vertical ozone flux above the RSL (especially prior to irrigation where $F_{O_3} \cong 0$) is due to the slight negative ozone gradient between the two upper-most mixing ratios (23 and 14 m) (Fig. 3). The negative gradient well above the canopy can be related to the stronger vertical mixing induced by the canopy (Harman and

Table 1. Ratio of estimated and observed u_* and sensible heat.

	u_*			H		
	MOST	MOST + RSL	Δ [%]	MOST	MOST + RSL	Δ [%]
Pre-irrigation	0.69	**0.80**	11	0.40	**0.61**	21
Post-irrigation	0.78	**0.90**	12	0.52	**0.81**	29

Mean estimates of u_* and sensible heat were calculated by the MOST and MOST + RSL methods at $1.25\,h_c$ within 10-17 LT for the pre- and post-irrigation periods; Δ represents the resulting difference between the ratio estimate of MOST + RSL and MOST values with respect to the K_COBS method in percentage.

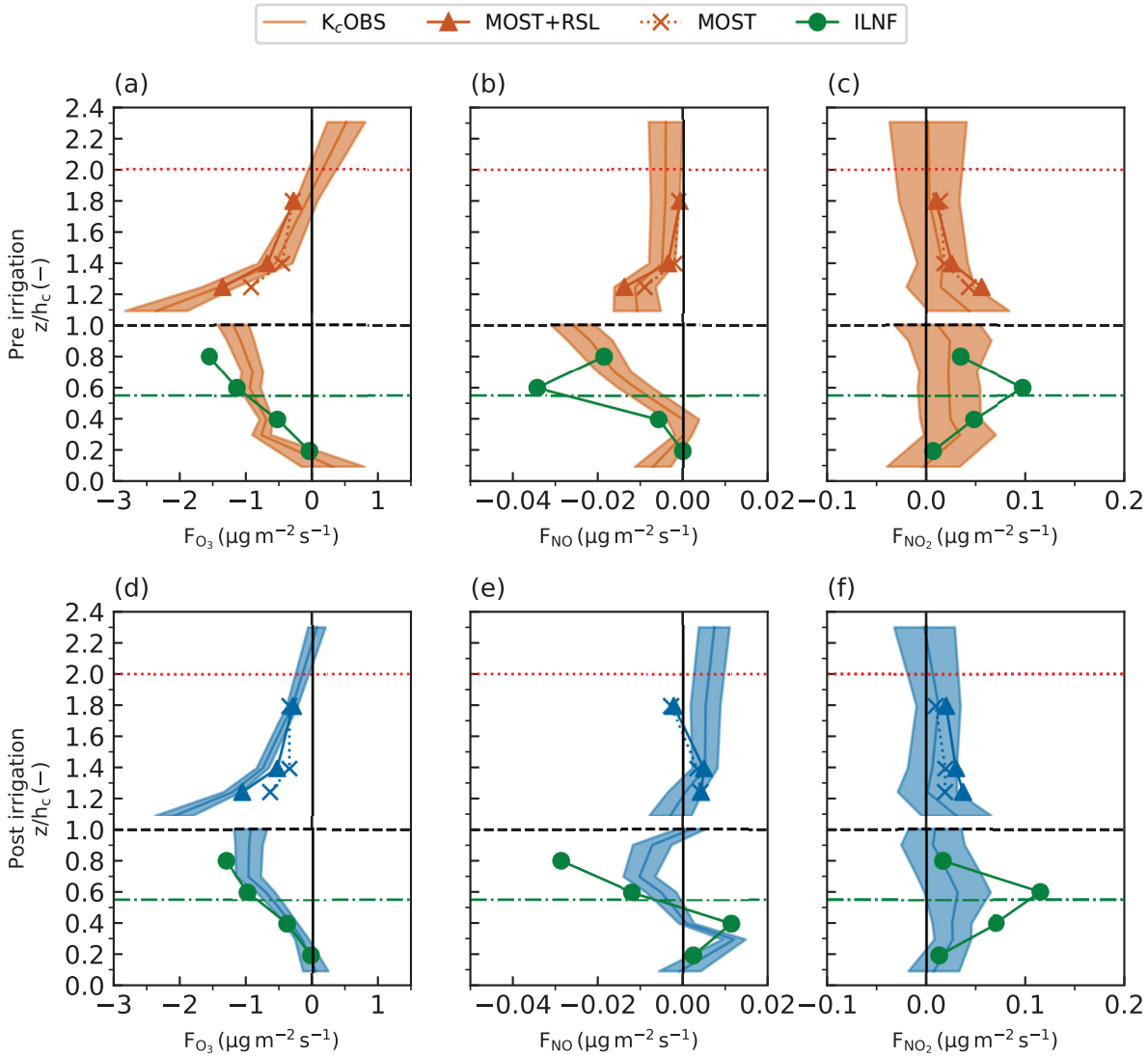

Fig. 6. Mean vertical profile of fluxes of (a, d) O_3, (b, e) NO and (c, f) NO_2 calculated via the K_cOBS, MOST, MOST + RSL and ILNF methods, averaged for the pre-and post-irrigation periods (pre irrigation top row, post irrigation bottom row), between 10:00 and 17:00 LT. See Fig. 3 for a description of the shaded area and horizontal lines.

Finnigan, 2007, 2008; Shapkalijevski et al., 2016), transporting scalars (ozone) upwards, and leading to maximum value of the ozone mixing ratio at 14 m. Another reason for the ozone mixing-ratio inflection point at 14 m is due to chemically produced ozone via (O_3-NO_2-NO) photolysis near the canopy, since both NO_2 and NO have an inflection point at the same level (Fig. 3b, c).

NO shows negative fluxes within the canopy before irrigation (Fig. 6b). Following irrigation there is a positive flux of NO at 0.3 m which may indicate increased soil emissions following soil wetting (Fig. 6e). Above the canopy, NO fluxes are negative before irrigation, with positive fluxes following irrigation, again indicating that NO soil emissions may have increased (Fig. 6b, e). NO_2 do not show this difference in fluxes between irrigation periods. NO_2 fluxes are positive throughout and above the canopy, tending to zero at 23 m (Fig. 6c, d).

The low intensity of turbulent mixing within the canopy, as quantified by the eddy diffusivity of momentum and heat in Fig. 5, suggests that other effects (e.g. chemistry) become more dominant than the vertical ozone exchange. Considering the photostationary state NO + O_3 <-> NO_2, one would expect that there will be less light in the canopy, shifting the equilibrium in the reaction to the right, with an 'apparent' positive flux of NO_2 (chemical production during transport) and negative fluxes for

Table 2. Ratio of mean fluxes calculated by MOST or MOST + RSL compared to fluxes calculated by the K_COBS method at $1.25\,h_c$ for the three main species, averaged within 10–17 LT.

	O_3			NO			NO_2		
	MOST	MOST + RSL	Δ [%]	MOST	MOST + RSL	Δ [%]	MOST	MOST + RSL	Δ [%]
Pre-irrigation	0.66	**0.97**	31	0.80	**0.82**	2	**2.95**	3.83	−88
Post-irrigation	0.53	**0.88**	35	**7.67**	7.93	−26	**14.97**	29.36	−1439

The bold numbers indicate the method performing closest to the K_COBS method; Δ represents the resulting difference between the ratio estimate of MOST+RSL and MOST values with respect to the K_COBS method in percentage.

NO and O_3. Qualitatively, this seems to correspond to the inferred fluxes in the canopy. Indeed, a major uncertainty when determining gas fluxes by all methods used in this study is the assumption of non-reactivity, which is discussed further in Section 5.1. As has been shown in a number of studies (e.g. Fitzjarrald and Lenschow, 1983; Kramm et al., 1991; Vila-Guerau De Arellano and Duynkerke, 1992), when chemical reactions have a similar timescale to turbulent mixing, this assumption may lead to erroneous flux calculation. In these cases, the vertical flux becomes a function of height due to chemical production or loss.

Table 2 gives an overview of the performance of the MOST + RSL and MOST method, relative to fluxes estimated by K_COBS for $1.25\,h_c$ for the three main chemical species considered. For O_3, the MOST + RSL method gives fluxes which are considerably closer to estimates by K_COBS, for both irrigation periods. However for NO and NO_2, the differences between flux estimated from the MOST and MOST + RSL methods are not easily explainable. A potential cause of this lack of agreement in flux estimation when using these methods for NO and NO_2 fluxes at CHATS is the small magnitude of NO_x fluxes, as well as the greater chemical reactivity of NO_x. This is discussed further in Section 5. Both MOST and MOST + RSL methods overestimated NO_2 fluxes before and after irrigation at the lower levels $z/h_c = 1.25$ and $z/h_c = 1.4$, and underestimated the NO fluxes at the highest level ($z/h_c = 1.8$) (Fig. 6).

In summary, the effects of the presence of tall canopy on ozone vertical exchange are twofold. Firstly, the canopy-induced turbulent mixing enhanced the ozone deposition near the canopy top. This was quantified by the increased magnitude of the vertical ozone flux (31% prior irrigation) and 35% after irrigation) as calculated by the MOST + RSL method at 2.5 m above the canopy top, compared to the MOST method values which omitted these effects. Secondly, the canopy was a source for VOCs (Karl et al., 2008), which likely, in combination with the presence of NO_x and the overall insufficient turbulent mixing, contributed to increased divergence in the ozone vertical flux profile.

4.3. Parameterizing gas deposition

As already mentioned before, deposition of O_3 is an important removal mechanism that needs to be represented in a parameterized form. Figure 7 shows derived O_3, NO and NO_2 deposition velocities (v_d) for both irrigation periods. The deposition velocity (cm s^{-1}) is calculated by:

$$v_d(z) = -\frac{F_C(z)}{[\overline{C}(z)]} \tag{8}$$

where $[\overline{C}]$ is the mixing ratio of a chemical species at height z. The largest O_3 deposition velocity is observed at the canopy-atmosphere interface ($z/h_c = 1.1$), with a maximum value of around 2 cm s^{-1} following irrigation. Thus, within the RSL, the canopy is acting as a sink for ozone. While NO shows the same signs of deposition velocity as O_3, NO_2 shows a reversed sign, with a minimum at the canopy top (Fig. 7). It is important to stress the large variation in deposition velocities with height. This result indicates the need to treat turbulent mixing within and above the canopy differently for chemically reactive species. As shown by Fig. 6e, the turbulent fluxes of NO change sign near the canopy sources and sinks. This indicates the need of more complete parameterizations than Eq. 8 to include the interaction between the canopy-turbulent effects and chemical transformations (Vila et al., 2004).

5. Discussion

5.1. Assumption of non-reactivity exchange coefficients

As mentioned above, a major uncertainty when determining gas fluxes by all methods used in this study is that these methods are based on the assumption that reactivity does not alter the turbulent eddy diffusivity. Under conditions when chemical reactions have a similar time scale to turbulence the vertical flux becomes a function of height due to chemical production or loss and the flux-profile relationships require modification. In high canopies, Patton et al. (2001) identified a large flux divergence for idealised decaying species, with a peak in this

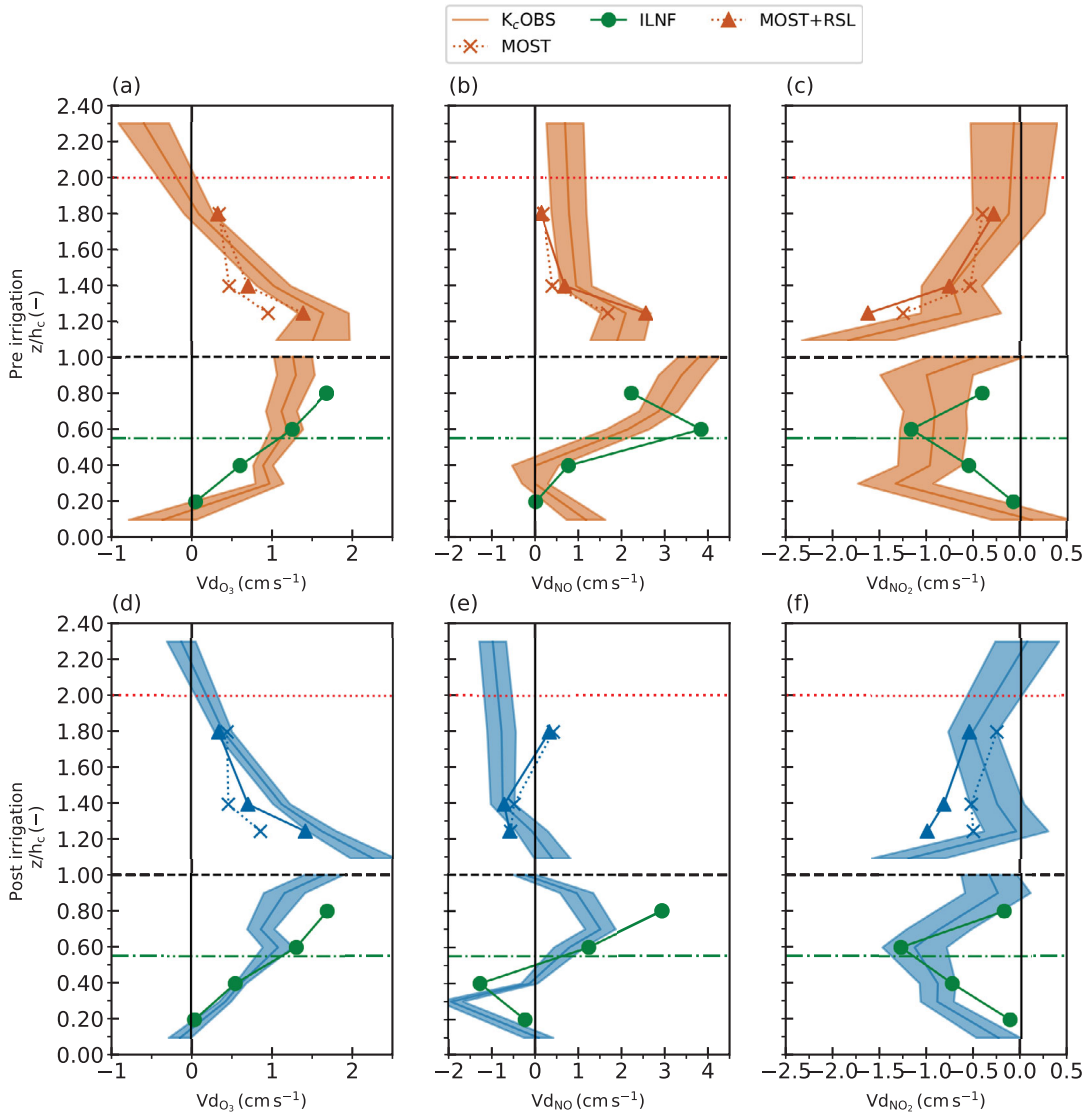

Fig. 7. Vertical profile of the deposition velocity of (a, b) O_3, (c, d) NO and (e, f) NO_2 calculated via the K_cOBS, MOST, MOST + RSL and ILNF methods, averaged for the pre-and post-irrigation periods, between 10:00 to 17:00 LT. See Fig. 3 for a description of the shaded area and horizontal lines.

divergence at the canopy top (Patton et al. 2001, Fig. 5b). To qualitatively see whether this assumption of non-reactivity is applicable to CHATS we can compare estimates of the time-scale of turbulence and chemical reactions. When the time scale of chemistry approaches the time scale of turbulent mixing, atmospheric turbulence can influence chemical reactivity (Vila et al., 2004). This leads to fluxes of chemically reactive species diverging from fluxes of inert scalars. By examining the reactive time scale and turbulent time scale at CHATS we can qualitatively say whether the assumption of a non-reactivity K-theory is valid. The primary pathway for boundary-layer O_3 production is through the photochemical reactions of NO_x, with these reactions rapidly reaching dynamic equilibrium in sunlight conditions (Griffin et al., 2007). The interconversion between O_3 and NO_x constitutes a chemical null cycle but acts to partition the chemical species:

$$NO + O_3 \xrightarrow{k1} NO_2 + O_2 \qquad (R1)$$

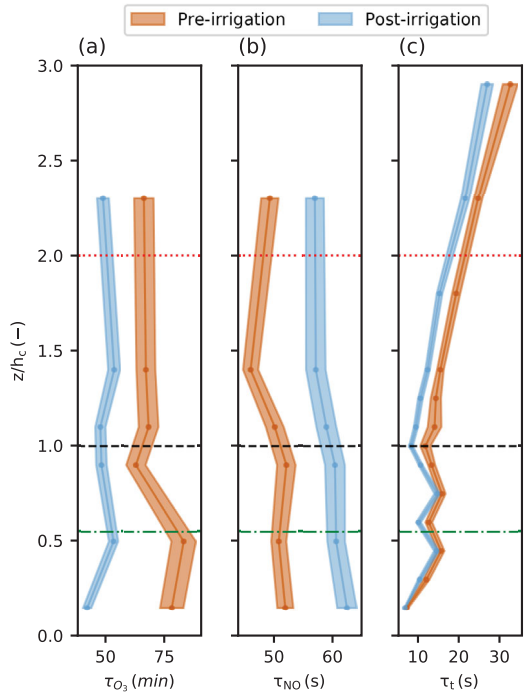

Fig. 8. Vertical profile of (a) τ_{O_3}, (b) τ_{NO} and (c) τ_t for the pre- and post-irrigation periods, averaged between 10:00 to 17:00 LT. Please note that τ_{O_3} is in minutes, while τ_{NO} and τ_t are in seconds. See Fig. 3 for a explanation of the three horizontal dashed lines.

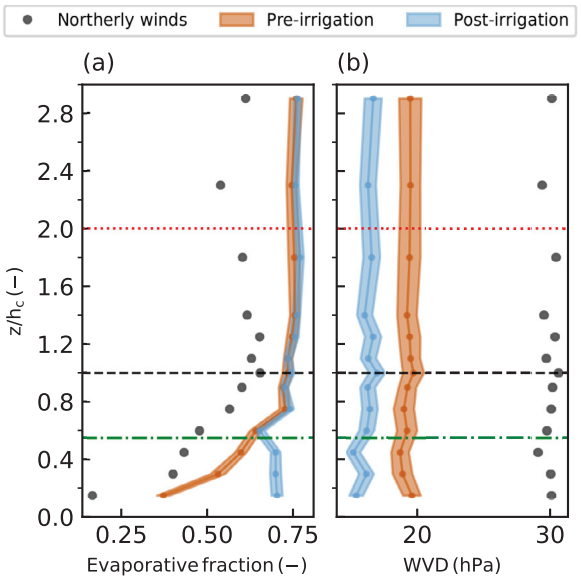

Fig. 9. Vertical profile of (a) evaporative fraction and, (b) water vapour deficit averaged between 10- 17 LT for the pre and post irrigation periods. See Figure 3 for an explanation of the horizontal lines.

$$NO_2 + h\nu \rightarrow NO + O_3 \quad \text{(R2)}$$

where $k_1 = 7.38 \cdot 10^{-2} \cdot \exp^{-1500/T}$ is the temperature (K) dependent second-order reaction rate (ppb s^{-1}) (Vilà-Guerau De Arellano et al., 2015). Deviations from this null cycle occur when reactions other than R1 convert NO to NO_2, with a major pathway being the reaction between VOC oxidation products and NO (Griffin et al., 2007).

To estimate a reactive time-scale for O_3 at the CHATS site, we can use:

$$\tau_{O_3} = \frac{1}{k_1[NO]} \quad (9)$$

The time-scale for NO (τ_{NO}) is calculated in a similar method as for τ_{O_3}. The time-scale of turbulence (τ_t) in the atmospheric surface layer is calculated via:

$$\tau_t = \frac{\kappa z}{u_*(z)} \quad (10)$$

Figure 8 shows the vertical profile of τ_{O_3}, τ_{NO} and τ_t for the pre-and post-irrigation periods. τ_{O_3} is in the order of minutes, while τ_{NO} and τ_t are in seconds. τ_t reaches a maximum of 30 s at 29 m. This calculation of τ_{O_3} is subject to a large amount of uncertainty given we are only considering the contribution of one reaction to the consumption of O_3. However given the large magnitude of difference between τ_{O_3} and τ_t, the assumption of non-reactivity can be considered to be valid for O_3. As τ_{NO} is of a similar magnitude to τ_t, fluxes of NO calculated using the inert K-theory must be treated more cautiously. The timescale of NO_2 varies diurnally with solar irradiance, with Calvert and Stockwell (1983) giving a timescale of 37.2 s for midday (Z (solar elevation) = 16.9°, sea level, assumed 0.20 albedo). Several studies have shown that NO shows the largest departure from inert K-theory when considering O_3-NO-NO_2 chemistry (e.g. Fitzjarrald and Lenschow, 1983; Gao et al., 1991; Vila-Guerau De Arellano and Duynkerke, 1992). For example, Vila-Guerau De Arellano and Duynkerke (1992) found that in neutral conditions NO departs from the inert K theory by 30% while NO_2 and O_3 departures by 5% and 3% respectively. Thus, the assumption that ozone acts as a passive tracer within and above the canopy can be considered valid when calculating ozone fluxes from vertical ozone gradients at CHATS. Fluxes of NO and NO_2 must be interpreted carefully, and their calculation will require a modification of Eq. (4) to include the effect of chemical transformation during the turbulent transport of these reactants (Vila-Guerau De Arellano and Duynkerke, 1992).

5.2. Irrigation influence

As seen in Figs. 2a and 3a, the mixing ratios of O_3 show a variation of ~8 ppb between the irrigation periods, a difference which is consistently maintained within and above the canopy. We have not found a significant change to O_3 fluxes (e.g. 4% at $z/h_c = 1.25$) before and after irrigation though (Fig. 6; Table 2). Since large-scale (Section 3) and local meteorological conditions (Fig. 3) vary between the irrigation periods, it is logical to hypothesize that the boundary-layer dynamics and the canopy (and soil moisture) conditions contributed to the changes in O_3 mixing ratios. Here we discuss the possible links between boundary-layer dynamics, canopy conditions, and O_3 mixing ratios and fluxes.

The difference in O_3 mixing ratios may be due to changes in water availability and plant stress. One link between plant stress and O_3 mixing ratios is the emission of VOCs. VOCs act as O_3 precursors and are often emitted by plants due to abiotic and biotic stresses (Karl et al., 2008). For example, significant amounts of MeSA were observed at the CHATS site (Karl et al., 2008). MeSA is a biologically active compound which is thought to be synthesized by plants as a response to temperature stress (Karl et al., 2008). Karl et al. (2008) found a correlation between differences in daytime maximum and night-time minimum temperatures and MeSA mixing ratios at the CHATS site and suggested that temperature stress, enhanced by drought stress may lead to MeSA emissions. Figure 3d also showed that the average mixing ratio of the total VOCs (including the MeSA), within and above the canopy, were consistently higher before the irrigation compared to after the irrigation. The warmer (about one degree) and drier (up to 2 g kg^{-1}) boundary layer conditions prior irrigation, compared to after irrigation (Fig. 3g, h), were in line with the increased VOCs pre-irrigation. To quantify the extent of water stress before and after irrigation on soil and vegetation, we calculated the evaporative fraction (EF) and the water vapour deficit (WVD) (Fig. 9). The evaporative fraction is the ratio between latent heat (LE) and the sum of latent and sensible heat ('EF = LE/H + LE'). There was a limited difference between the EF above the canopy before and after irrigation, while there was a sharp decline in EF below the canopy before irrigation (Fig. 9a). While the canopy can maintain a constant water content through stomatal regulation and deep roots, the soil dried out rapidly leading to a low EF below the canopy. Thus, prior to irrigation the only source of water vapour was the canopy (leading to a low EF in the sub-canopy layer), whereas after irrigation, the soil became an important source of water vapour as well. The WVD is higher by 5 hPa before irrigation. This is supported by Karl et al. (2008) who found that the trees at the CHATS site were forced to reduce water loss due to water stress prior to irrigation. This water stress is coupled with the increase in VOCs mixing ratios before irrigation (Figs. 2d and 3d), suggesting that the water stress may trigger chemical reactions other that R1 and R2, resulting in O_3 production.

Additionally, dry conditions can contribute to stomatal closure, which can decrease O_3 deposition. As a consequence, this can increase O_3 mixing ratios. Fares et al. (2014) concluded that stomatal closure due to the high WVD and low soil water content leads to low O_3 deposition fluxes. Our analysis, showed no clear evidence for stomatal closure at the CHATS orchard before irrigation, since in addition to the lack of difference in EF between the irrigation periods (in the canopy layer), there was also no significant difference in the average calculated CO_2 fluxes (not shown here). Thus, we presume that there are very limited changes in the stomatal deposition of O_3 pre and post irrigation.

On the other hand, the irrigation contributed to increased evaporation by soil (in the sub-canopy layer, Fig. 9a), and NO soil emissions, especially in the sub-canopy layer and above the canopy (Fig. 6e). During this period (post-irrigation), the total VOCs mixing ratios were decreased for about 1.5 ppb (or 27%) on average (Fig. 3d). This emission of NO by the soil, as well as the increased surface wetness of the soil after irrigation could potentially contribute the altered chemistry (Lamaud et al., 2002) and ozone deposition onto soil (Fares et al., 2012). The latter however is likely not the case since no significant signals of enhanced post-irrigation ozone deposition are found (Fig. 6a, d).

The local effects of water availability and plant stress in the orchard may have influenced the change in O_3 mixing ratios and the chemical regime, but the effects of larger scales remain relevant when studying the local O_3 budget. It has been demonstrated that the CHATS boundary-layer thermodynamics and chemical composition is largely controlled by the horizontal transport of heat, moisture, and chemical constituents (Fujita et al., 2005; Bao et al., 2008; Bianco et al., 2011; Shapkalijevski et al., 2017). The horizontal advection of air with an altered ratio of O_3 precursors may lead to a change in the O_3 production regime. As the area to the south of the orchard was a busy highway, the predominate wind regime will advect NO_x polluted air. Opposite to that, during the" northerly winds" period there was a clear wind regime shift, with the winds shifting to the north and advecting warm, dry air while suppressing the morning NO_x mixing ratio peaks (Figs. 1–3).

It is important to mentioning here the nonlinearity of ozone formation for a given variety of NO_x conditions

(Jacob, 1999). Depending on the concentration levels, NO_x may either lead to ozone production (via VOCs $\rightarrow$ $RO_2 + NO \rightarrow NO_2 \rightarrow O_3$ or to ozone destruction (i.e. $NO + O_3 \rightarrow NO_2$ (+ OH) $\rightarrow HNO_3$) (Rohrer and Berresheim, 2006). Due to the highly non-linear relations of the O_3-NO_x-VOC system (Sillman et al., 1990), and having in mind the limitation in the observational data we have, we are inconclusive whether the variations of O_3 are locally driven, or dominated by larger-scale processes; or perhaps combination of both.

6. Conclusions

We have presented the micrometeorological and chemical characteristics observed at the Canopy Horizontal Array Turbulence Study (CHATS) site. Based on the CHATS comprehensive data set, we have investigated state-of-the-art representation of the roughness sub-layer above a tall canopy influence the estimations of the O_3 vertical exchange and O_3 deposition. The period under study includes full irrigation cycle, which enables us to analyze how O_3 mixing ratio are influence by water (non)availability.

Our main focus was on quantifying the effect of the orchard canopy at CHATS on ozone (O_3) vertical exchange. To account for the effects of the canopy-induced turbulent mixing on ozone vertical exchange we have calculated the ozone vertical fluxes from O_3 mixing ratio gradients above the canopy by using a flux-gradient method with roughness-sublayer (RSL) parameterization, as opposed to the standard flux-gradient method. The validation of this methodology was provided by calculating the friction velocity and the sensible flux, for which direct flux measurements using EC were available. We found that, by including a parametrization for the RSL, the friction velocity and sensible heat flux estimates were improved for up to 12 and 29%, respectively, at 2.5 m above the canopy top, with sensible heat flux estimated within minimum of 61% of observations. When considering estimates of fluxes of chemically-reactive compounds, including the parametrization for the RSL improved the estimated O_3 fluxes relative to fluxes estimated using a locally derived turbulent transfer coefficient. The 35% increased ozone deposition flux, calculated including the RSL parameterization above the canopy (at 2.5 m above the canopy top), represents the contribution of the canopy-induced turbulent mixing on the ozone vertical exchange. Our results indicate that including the parametrization for the influence of the RSL on turbulent mixing has the potential to provide increased accuracy when estimating above-canopy O_3 fluxes, and will be especially useful for improving estimations of O_3 deposition to vegetation. Consequently, this method (RSL modification) can be a useful tool when investing the influence of the tall canopy on ozone exchange.

We have also investigated and discussed the influence of the water stress on the differences in O_3 mixing ratios before and after irrigation periods at this rural Californian orchard. Significantly higher O_3 (up to 8 ppb) as well as total biogenic VOCs (up to 1.5 ppb) mixing ratios were found prior to irrigation compared to after irrigation. These mixing ratio decreases following irrigation did not typically result in significant changes to average fluxes between irrigation periods. Our analysis indicated that the observed larger O_3 mixing ratio prior the irrigation were likely due to the combined effects of local-scale VOCs emissions, induced by water stress, and the boundary-layer meteorological conditions. Opposite to that, we also found a strong negative vertical divergence of the ozone flux in the canopy layer and the RSL for both, pre-, and post-irrigation periods, indicating that the canopy was a sink of ozone. We hypnotize that the volatile organic compounds (VOCs) with short lifetime (e.g. monoterpenes), together with the presence of NO_x are responsible for the chemical losses of O_3. However, more complete measurement set of chemistry, including these fast reactive VOCs would be needed to verify this in-canopy chemistry.

Acknowledgements

The authors gratefully acknowledge the provision of the high quality meteorological and chemistry data by the Canopy Horizontal Array Turbulence Study (CHATS) community.

References

Baldocchi, D., Falge, E., Gu, L., Olson, R., Hollinger, D. and co-authors. 2001. FLUXNET: a new tool to study the temporal and spatial variability of ecosystem–scale carbon dioxide, water vapor, and energy flux densities. *Bull. Am. Meteorol. Soc.* **82**, 2415–2434. doi:10.1175/1520-0477(2001)082<2415:FANTTS>2.3.CO;2

Bao, J.-W., Michelson, S. A., Persson, P. O. G., Djalalova, I. V., Wilczak, J. M. and co-authors. 2008. Observed and WRF-simulated low-level winds in a high-ozone episode during the Central California Ozone Study. *J. Appl. Meteorol. Climatol.* **47**, 2372–2394. doi:10.1175/2008JAMC1822.1

Bianco, L., Djalalova, I. V., King, C. W. and Wilczak, J. M. 2011. Diurnal evolution and annual variability of boundary-layer height and its correlation to other meteorological variables in California's central valley. *Boundary Layer Meteorol.* **140**, 491–511. doi:10.1007/s10546-011-9622-4

Bonan, G. B. 2008. Forests and climate change: forcings, feedbacks, and the climate benefits of forests. *Science* **320**, 1444–1449. doi:10.1126/science.1155121

Calvert, J. G. and Stockwell, W. R. 1983. Deviations from the O 3 –NO–NO 2 photostationary state in tropospheric chemistry. *Can. J. Chem.* **61**, 983–992. doi:10.1139/v83-174

Cellier, P. and Brunet, Y. 1992. Flux-gradient relationships above tall plant canopies. *Agric. For. Meteorol.* **58**, 93–117. 90113-I. doi:10.1016/0168-1923(92)90113-I

De Ridder, K. 2010. Bulk transfer relations for the roughness sublayer. *Boundary Layer Meteorol.* **134**, 257–267. doi:10.1007/s10546-009-9450-y

Denmead, O. T. and Bradley, E. F. 1987. On scalar transport in plant canopies. *Irrig. Sci.* **8**, 131–149.

Dupont, S. and Patton, E. G. 2012. Momentum and scalar transport within a vegetation canopy following atmospheric stability and seasonal canopy changes: The CHATS experiment. *Atmos. Chem. Phys.* **12**, 5913–5935. doi:10.5194/acp-12-5913-2012

Fares, S., Savi, F., Muller, J., Matteucci, G. and Paoletti, E. 2014. Simultaneous measurements of above and below canopy ozone fluxes help partitioning ozone deposition between its various sinks in a Mediterranean Oak Forest. *Agric. For. Meteorol.* **198–199**, 181–191. doi:10.1016/j.agrformet.2014.08.014

Fares, S., Weber, R., Park, J.-H., Gentner, D., Karlik, J., and co-authors. 2012. Ozone deposition to an orange orchard: Partitioning between stomatal and non-stomatal sinks. *Environ. Pollut.* **169**, 258–266. doi:10.1016/j.envpol.2012.01.030

Finnigan, J. J., Shaw, R. H. and Patton, E. G. 2009. Turbulence structure above a vegetation canopy. *J. Fluid Mech.* **637**, 387–424. doi:10.1017/S0022112009990589

Fitzjarrald, D. R. and Lenschow, D. H. 1983. Mean concentration and flux profiles for chemically reactive species in the atmospheric surface layer. *Atmospheric Environ.* **17**, 2505–2512. doi:10.1016/0004-6981(83)90076-8

Fujita, E. M., Campbell, D. E. and Snorradottir, T. 2005. *Central California Ozone Study (CCOS) Data Validation. Final Report, California Air Resources Board, Sacramento, CA.* Technical Report, California Air Resources Board, Sacramento, CA. Online at http://www.arb.ca.gov/airways/ccos/ccos.htm

Gao, W., Shaw, R. H. and Paw, K. T. 1989. Observation of organized structure in turbulent flow within and above a forest canopy. In: *Boundary Layer Studies and Applications*. Springer, Netherlands, pp. 349–377.

Gao, W., Wesely, M. L. and Lee, I. Y. 1991. A numerical study of the effects of air chemistry on fluxes of NO, NO2, and O3 near the surface. *J. Geophys. Res.* **96**, 18761–18769. doi:10.1029/91JD02106

Garratt, J. R. 1980. Surface influence upon vertical profiles in the atmospheric near-surface layer. *Q. J. R. Meteorol. Soc.* **106**, 803–819. doi:10.1002/qj.49710645011

Gerken, T., Chamecki, M. and Fuentes, J. D. 2017. Air-parcel residence times within forest canopies. *Boundary Layer Meteorol.* **165**, 29–54. 1007/s10546-017-0269-7. doi:10.1007/s10546-017-0269-7

Griffin, R. J., Beckman, P. J., Talbot, R. W., Sive, B. C., Varner, R. K. and co-authors. 2007. Deviations from ozone photostationary state during the International Consortium for Atmospheric Research on Transport and Transformation 2004 campaign: Use of measurements and photochemical modeling to assess potential causes. *J. Geophys. Res. Atmos.* **112**, D10S07.

Harman, I. N. and Finnigan, J. J. 2007. A simple unified theory for flow in the canopy and roughness sublayer. *Boundary Layer Meteorol.* **123**, 339–363. doi:10.1007/s10546-006-9145-6

Harman, I. N. and Finnigan, J. J. 2008. Scalar concentration profiles in the canopy and roughness sublayer. *Boundary Layer Meteorol.* **129**, 323–351. doi:10.1007/s10546-008-9328-4

Högström, U. 1988. Non-dimensional wind and temperature profiles in the atmospheric surface layer: a re-evaluation. In: *Topics in Micrometeorology. A Festschrift for Arch Dyer*. Springer, pp. 55–78.

Iwata, H., Harazono, Y. and Ueyama, M. 2010. Influence of source/sink distributions on flux gradient relationships in the roughness sublayer over an open forest canopy under unstable conditions. *Boundary Layer Meteorol.* **136**, 391–405. doi:10.1007/s10546-010-9513-0

Jacob, D. 1999. *Introduction to Atmospheric Chemistry*. New Jersey, US: Princeton University Press, p. 280.

Jacobson, M. Z. 2005. *Fundamentals of Atmospheric Modeling*. Cambridge: Cambridge University Press.

Karl, T., Guenther, A., Turnipseed, A., Patton, E. G. and Jardine, K. 2008. Chemical sensing of plant stress at the ecosystem scale". English. *Biogeosciences* **5**, 1287–1294. doi:10.5194/bg-5-1287-2008

Kramm, G., Müller, H., Fowler, D., Höfken, K. D., Meixner, F. X. and co-authors. 1991. A modified profile method for determining the vertical fluxes of NO, NO2, ozone, and HN03 in the atmospheric surface layer. *J. Atmos. Chem.* **13**, 265–288. doi:10.1007/BF00058135

Lamaud, E., Carrara, A., Brunet, Y., Lopez, A. and Druilhet, A. 2002. Ozone fluxes above and within a pine forest canopy in dry and wet conditions. *Atmos. Environ.* **36**, 77–88. doi:10.1016/S1352-2310(01)00468-X

Min, K. E., Pusede, S. E., Browne, E. C., LaFranchi, B. W. and Cohen, R. C. 2014. Eddy covariance fluxes and vertical concentration gradient measurements of NO and NO2 over a ponderosa pine ecosystem: observational evidence for within-canopy chemical removal of NOx. *Atmos. Chem. Phys.* **14**, 5495–5512. doi:10.5194/acp-14-5495-2014

Moene, F. A. and Van Dam, C. J. 2014. *Transport in the Atmosphere-Vegetation-Soil Continuum*. New York, NY: Cambridge University Press.

Mölder, M., Grelle, A., Lindroth, A. and Halldin, S. 1999. Flux-profile relationships over a boreal forest—roughness sublayer corrections. *Agric. For. Meteorol.* **98**, 645–658.

Monin, A. S. and Obukhov, A. M. 1954. Basic laws of turbulent mixing in the surface layer of the atmosphere. *Inst. Contract Number* **24**, 163–187.

Murphy, J. G., Day, D. A., Cleary, P. A., Wooldridge, P. J., Millet, D. B. and co-authors. 2007. The weekend effect within and downwind of Sacramento – Part 1: Observations of ozone, nitrogen oxides, and VOC reactivity. *Atmos. Chem. Phys.* **7**, 5327–5339. doi:10.5194/acp-7-5327-2007

Patton, E. G., Davis, K. J., Barth, M. C. and Sullivan, P. P. 2001. Decaying scalars emitted by a forest canopy: a

numerical study. *Boundary Layer Meteorol.* **100**, 91–129. doi:10.1023/A:1019223515444

Patton, E. G., Horst, T. W., Sullivan, P. P., Lenschow, D. H., Oncley, S. P. and co-authors. 2011. The canopy horizontal array turbulence study. *Bull. Am. Meteorol. Soc.* **92**, 593–611. 1. doi:10.1175/2010BAMS2614.1

Paulson, C. A. 1970. The mathematical representation of wind speed and temperature profiles in the unstable atmospheric surface layer. *J. Appl. Meteorol.* **9**, 857–861. doi:10.1175/1520-0450(1970)009<0857:TMROWS>2.0.CO;2

Physick, W. L. and Garratt, J. R. 1995. Incorporation of a high-roughness lower boundary into a mesoscale model for studies of dry deposition over complex terrain. *Boundary Layer Meteorol.* **74**, 55–71. doi:10.1007/BF00715710

Raupach, M. R. 1979. Anomalies in flux-gradient relationships over forest. *Boundary Layer Meteorol.* **16**, 467–486. doi:10.1007/BF03335385

Raupach, M. R. 1989a. Applying Lagrangian fluid mechanics to infer scalar source distributions from concentration profiles in plant canopies. *Agric. For. Meteorol.* **47**, 85–108. doi:10.1016/0168-1923(89)90089-0

Raupach, M. R. 1989b. A practical Lagrangian method for relating scalar concentrations to source distributions in vegetation canopies. *Q. J. R. Meteorol. Soc.* **115**, 609–632. doi:10.1002/qj.49711548710

Raupach, M. R., Finnigan, J. J. and Brunei, Y. 1996. Coherent eddies and turbulence in vegetation canopies: the mixing-layer analogy. *Boundary Layer Meteorol.* **78**, 351–382. doi:10.1007/BF00120941

Rohrer, F. and Berresheim, H. 2006. Strong correlation between levels of tropospheric hydroxyl radicals and solar ultraviolet radiation. *Nature* **442**, 184–187. doi:10.1038/nature04924

Seinfeld, J. H. and Pandis, S. N. 2016. *Atmospheric Chemistry and Physics: From Air Pollution to Climate Change.* New Jersey: John Wiley and Sons.

Seok, B., Helmig, D., Ganzeveld, L., Williams, M. W. and Vogel, C. S. 2013. Dynamics of nitrogen oxides and ozone above and within a mixed hardwood forest in northern Michigan. *Atmos. Chem. Phys.* **13**, 7301–7320. doi:10.5194/acp-13-7301-2013

Shapkalijevski, M., Moene, A. F., Ouwersloot, H. G., Patton, E. G. and Vilà-Guerau de Arellano, J. 2016. Influence of canopy seasonal changes on turbulence parameterization within the roughness sublayer over an orchard canopy. *J. Appl. Meteorol. Climatol.* **55**, 1391–1407. doi:10.1175/JAMC-D-15-0205.1

Shapkalijevski, M. M., Ouwersloot, H. G., Moene, A. F. and de Arrellano, J. V.-G. 2017. Integrating canopy and large-scale atmospheric effects in convective boundary layer dynamics during CHATS experiment. *Atmos. Chem. Phys.* **17**, 1623–1640. doi:10.5194/acp-17-1623-2017

Sillman, S., Logan, J. A. and Wofsy, S. C. 1990. The sensitivity of ozone to nitrogen oxides and hydrocarbons in regional ozone episodes. *J. Geophys. Res.* **95**, 1837–1851. doi:10.1029/JD095iD02p01837

Simard, M., Pinto, N., Fisher, J. B. and Baccini, A. C. G. 2011. Mapping forest canopy height globally with spaceborne lidar. *J. Geophys. Res.* **116**, G04021. doi:10.1029/2011JG001708

Stull, R. B. 1988. *An Introduction to Boundary Layer Meteorology.* Vol. 13. New York, US: Springer Science and Business Media, p. 670.

Thom, A. S., Stewart, J. B., Oliver, H. R. and Gash, J. H. C. 1975. Comparison of aerodynamic and energy budget estimates of fluxes over a pine forest. *Q. J. R. Meteorol. Soc.* **101**, 93–105. doi:10.1002/qj.49710142708

Vila, G. D., Arellano, J., Dosio, A., Vinuesa, J.-F., Holtslag, A. A. M. and co-authors. 2004. The dispersion of chemically reactive species in the atmospheric boundary layer. *Meteorol. Atmos. Phys.* **87**, 23–38. 0059–2.

Vila-Guerau De Arellano, J. and Duynkerke, P. G. 1992. Influence of chemistry on the flux-gradient relationships for the NO-O3-NO2 system. *Boundary Layer Meteorol.* **61**, 375–387. doi:10.1007/BF00119098

Vilà-Guerau De Arellano, J., van Heerwaarden, C. C., van Stratum, B. J. H. and van den Dries, K. 2015. *Atmospheric Boundary Layer: Integrating Chemistry and Land Interactions*. 1st ed. Cambridge, UK: Cambridge University Press, pp. 1–283.

Wilczak, J. M., Oncley, S. P. and Stage, S. A. 2001. Sonic anemometer tilt correction algorithms. *Boundary Layer Meteorol.* **99**, 127–150. doi:10.1023/A:1018966204465